1 **Phosphoproteomics reveals new insights into the role of PknG during the persistence of**

2 **pathogenic mycobacteria in host macrophages**

3 Seanantha S. Baros-Steyl[1], Kehilwe C. Nakedi[1], Tariq A. Ganief[1,2], Javan O. Okendo[1], David L.

4 Tabb[3,4,5], Nelson C. Soares[6,7]* and Jonathan M. Blackburn[1,2]*

5 [1] Division of Chemical & Systems Biology, Department of Integrative Biomedical Sciences,

6 Faculty of Health Sciences, University of Cape Town. South Africa.

7 [2] Institute of Infectious Disease & Molecular Medicine, Faculty of Health Sciences, University of

8 Cape Town. South Africa.

9 [3] Division of Molecular Biology and Human Genetics, Department of Biomedical Sciences,

10 Stellenbosch University, Cape Town, South Africa

11 [4] Bioinformatics Unit, South African Tuberculosis Bioinformatics Initiative, Stellenbosch

12 University, Cape Town, South Africa.

13 [5] South African Medical Research Council Centre for Tuberculosis Research, Stellenbosch

14 University, Cape Town, South Africa.

15 [6] Sharjah Institute for Medical Research, University of Sharjah, Sharjah, United Arab Emirates.

16 [7] College of Pharmacy, University of Sharjah, Sharjah, United Arab Emirates.

17 *** Correspondence**:

18 Prof. Jonathan M Blackburn

19 e-mail: jonathan.blackburn@uct.ac.za

20 Dr Nelson C Soares

21 e-mail: nsoares@sharjah.ac.ae

22 **Keywords: Mass spectrometry, Phosphoproteomics, Post-translational modifications,**

23 *Mycobacterium tuberculosis*, **Phosphorylation, Serine/Threonine Protein Kinases, Substrate**

24 **identification**

25   **Abstract**

26   Pathogenic mycobacteria, such as *Mycobacterium tuberculosis,* modulate the host immune system

27   to evade clearance and promote long-term persistence, resulting in disease progression or latent

28   infection. Understanding the mechanisms pathogenic mycobacteria use to escape elimination by

29   the host immune system is critical to better understanding the molecular mechanisms of

30   mycobacterial infection. Protein kinase G (PknG) in pathogenic mycobacteria has been shown to

31   play an important role in avoiding clearance by macrophages through blocking phagosome-

32   lysosome fusion; however, the exact mechanism is not completely understood. Here, to further

33   investigate the role of mycobacterial PknG during early events of macrophage infection, RAW

34   264.7 macrophage cell lines were infected with *M. bovis* BCG wild-type and PknG knock-out

35   mutant strains. After proteolysis, phosphopeptides were enriched via TiO_2 columns and subjected

36   to LC-MS/MS to identify differentially phosphorylated peptides between the wild-type and PknG

37   mutant infected macrophages. A total of 1401 phosphosites on 914 unique proteins were identified.

38   Following phosphoproteome normalisation and differential expression analysis, a total of 149

39   phosphosites were differentially phosphorylated in the wild-type infected RAW 264.7

40   macrophages versus the PknG knock-out mutant. A subset of 95 phosphosites was differentially

41   up-regulated in the presence of PknG. Functional analysis of our data revealed that PknG kinase

42   activity reprograms normal macrophage function through interfering with host cytoskeletal

43   organisation, spliceosomal machinery, translational initiation, and programmed cell death.

44   Differentially phosphorylated proteins in this study serve as a foundation for further validation and

45   PknG host substrate assignment.

46   **Importance**

47   Tuberculosis (TB) remains one of the leading causes of death from infection worldwide, due to

48   the ability of *Mycobacterium tuberculosis* (*Mtb*) to survive and replicate within the host,

49   establishing reservoirs of live bacteria that promote persistence and recurrence of disease.

50   Understanding the mechanisms that *Mtb* uses to evade the host immune system is thus a major

51   goal in the TB field. Protein kinase G is thought to play an important role in *Mtb* avoiding clearance

52   by the host through disruption of macrophage function, but the underlying molecular mechanisms

53   of this are not well understood. Here, our new phosphoproteomic data reveals that mycobacterial

54   PknG substantially reprograms normal macrophage function through extensive PknG-mediated

55   post-translational control of critical host cellular processes. These novel findings therefore

56   considerably increase our knowledge of mycobacterial pathogenicity, including specific host

57   cellular pathways that might be re-activatable through host-directed therapy, thereby restoring

58   macrophage ability to eliminate *Mtb*.

Introduction

Tuberculosis (TB) remains one of the leading causes of death from infection worldwide (1). The high prevalence of TB is due to the ability of *Mycobacterium tuberculosis (Mtb)* to survive and replicate within the alveolar macrophages, establishing reservoirs of live bacteria that promote persistence and recurrence of the disease. An estimated one-quarter of the global population harbours a latent TB infection (LTBI) (2), which, although asymptomatic, represent a reservoir for potential reactivation and transmission of TB (3).

Pathogenic mycobacteria suppress various host processes including phagosome-lysosome fusion, programmed cell death, and antigen presentation (4). In addition, *Mtb* promotes the activation of pathways involving mitogen-activated protein kinases (MAPKs), calcium signalling, and interferon-γ (IFN-γ) to weaken mycobactericidal responses (5, 6). Mycobacterial Ser/Thr protein kinases (STPKs) and phosphatases are known to play a role in interfering with host-signalling pathways during infection, thereby promoting intracellular survival (9–12).

The mycobacterial secretory protein kinase G (PknG) is a known virulence factor and contributes to the inhibition of phagosome-lysosomal fusion during early-stage infection (9). This is presumably a result of a kinase-mediated signalling mechanism through which PknG interacts/phosphorylates host protein substrates, thereby facilitating intracellular survival of the pathogen (9, 13). Experimental evidence shows that inactivation of PknG, either by gene disruption or chemical inhibition, results in lysosomal localisation and mycobacterial cell death in infected macrophages (9, 13). Although these processes are seemingly dependent on the kinase activity of PknG, the exact mechanism that PknG employs to establish a niche inside host macrophages remains unclear. Thus, understanding the mechanistic connection between PknG in such complex

81   regulatory signalling networks and mycobacterial survival in macrophages requires a detailed view

82   of the phosphorylation events taking place at a given time during infection.

83   Our previous *in vivo* study identified novel mycobacterial physiological substrates for PknG by

84   comparing the phosphoproteome dynamics during growth in liquid culture of *M. bovis* BCG wild-

85   type (WT) against the respective PknG knock-out (ΔPknG) mutant (14). The study revealed a new

86   set of protein targets that were seen to be exclusively phosphorylated in *M. bovis* BCG WT and

87   not in the ΔPknG mutant. Further validation of these initial results using PRMs and docking

88   analyses allowed the identification of a set of mycobacterial proteins as novel physiological

89   substrates for PknG (14).

90   Here, by employing a similar strategy, we aim to extend our knowledge of mycobacterial

91   Ser/Thr/Tyr phosphorylation networks to *M. bovis* BCG-infected macrophages. Initial events

92   during infection of host cells by pathogens can guide the overall course of infection and determine

93   its eventual outcome. To understand host-pathogen interactions during this early stage of infection

94   at the post-translational level, we analysed changes in the phosphoproteome of RAW 264.7

95   macrophage cells after infection with *M. bovis* BCG WT against those infected with the ΔPknG

96   mutant. Through this work, we identify plausible protein phosphorylation mechanisms by which

97   pathogenic mycobacterial PknG interferes with macrophage function to promote mycobacterial

98   survival.

99   **Materials and Methods**

100   *M. bovis BCG strains and bacterial culture*

101   Bacterial strains used in this study were kindly donated by Professor Jean Pieters, University of

102   Basel, Switzerland. The mutant (*M. bovis* BCG ΔPknG) was generated as described in Walburger

103 et. al. (2004) (9). Mycobacteria were grown in 7H9 Middlebrook (BD, Maryland, USA) broth

104 supplemented with 0.05% Tween 80, OADC (Becton Dickinson) and 0.2 % (v/v) glycerol. The

105 cells were grown at 37 ⁰C with continuous agitation (120 rpm). Growth was monitored daily by

106 measuring the optical density (OD_{600}) until the desired OD was reached.

107 *Culture conditions of RAW 264.7 macrophages*

108 The murine macrophage cell line RAW 264.7 was used to study the host-pathogen interactions in

109 this study. Murine macrophages have been used as a successful model to study host-pathogen

110 interaction in *Mtb* studies. Our stocks were kindly donated by one of our collaborators from the

111 University of Stellenbosch. Frozen stocks of the cell lines were defrosted at 37°C in a water bath.

112 The cells in suspension were pelleted by centrifugation at 800 x g for 3 minutes. The cell pellets

113 were washed twice with pre-warmed PBS and pelleted. The pellets were re-suspended in

114 Dulbecco's modified Eagle medium (DMEM) (Difco), supplemented with pyruvate and glutamine

115 (Difco) and 10% (v/v) heat-inactivated foetal calf serum (FCS) (Sigma-Aldrich) (D10). The cells

116 were then seeded into T25 tissue culture flasks (Lasec, South Africa) at 30% confluence and grown

117 in a humidified (95%) incubator at 37°C with 5% CO_2.

118 *Infection of macrophages with M. bovis BCG strains*

119 Bacterial cells, at the desired OD based on the multiplicity of infection (MOI), were washed twice

120 with PBS, and D10 was added to the cell pellet. Bacterial clumps were minimised using a water

121 bath sonicator for 10 minutes. Bacterial cells were also passed through a needle 10 times using a

122 10 mL syringe, followed by gentle centrifugation (1000 x g for 5 min) to sediment clumps.

123 Macrophage media was removed and washed twice with pre-warmed PBS and replaced with

124 bacteria in D10 at MOI 1:4. Cells were incubated for 30 minutes uptake and washed five times

125 with PBS. Fresh D10 was then added and incubated for a further 30 minutes and harvested. A

126   modified RIPA buffer was added to the cells and agitated for 5 minutes on ice prior to treatment

127   with endonuclease benzonase (Sigma).

128   *Tryptic digestion and phosphopeptide enrichment*

129   In-solution digestion was carried out on 500 µg total protein. Briefly, proteins were denatured with

130   1 mM dithiothreitol (DTT) for 1 hour at room temperature with gentle agitation and alkylated with

131   5.5 mM iodoacetamide (IAA) for 1 hour in the dark. Proteins were pre-digested with Lys-C

132   endopeptidase (Wako, Neuss, Germany) for 3 hours at 30°C before being diluted four times with

133   HPLC-grade water to a final concentration of ~1.5 M urea. The diluted sample was then digested

134   overnight with trypsin (1:100 ratio) at 30°C. The digestion was quenched with 1% trifluoroacetic

135   acid (TFA) (Sigma Aldrich, St Louis, USA).

136   Digested peptides were desalted using in-house reverse-phase C18 chromatography (Millipore) in

137   preparation for mass spectrometry (MS) analysis. Briefly, C18 columns were equilibrated twice

138   with solvent B [80% acetonitrile (ACN) and 0.1% formic acid (FA)] added and centrifuged at 3000

139   x g for 30 seconds. Samples were washed twice with solvent A (2% ACN and 0.1%FA) before

140   being added to the column. Peptides were eluted with solvent C (60% ACN and 0.1% FA) and

141   dried down at room temperature in a SpeedVac vacuum concentrator (Savant). 50 µg of protein

142   was reserved for proteome analysis and the rest enriched for phosphorylated peptides using a TiO_2

143   phosphopeptide enrichment kit (ThermoFischer Scientific) according to the manufacturer's

144   instructions.

145   *Liquid chromatography with tandem mass spectrometry (LC-MS/MS analysis)*

146   LC-MS/MS analysis was performed using the Dionex Ultimate 3500 RSLC Nano System (Thermo

147   Fisher Scientific) coupled to a Q Exactive mass spectrometer (Thermo Fisher Scientific). After

148   being desalted as described before, proteome and phosphoproteome peptides were resuspended in

149   15 µL of solvent A, of which 4 µL was loaded at 1 µg per injection into the LC-MS/MS system.

150   Peptides were chromatographically separated using a 75 µm (ID), 25 cm column packed in-house

151   with reversed-phase 3 µm Kinetex core-shell C18 resin (Phenomenex) at a flow rate of 400 nL/min

152   at 40°C. The gradient consisted of 2% solvent B (0.1% FA, ACN) increased to 8% solvent B over

153   2 minutes, followed by increasing to 23% solvent B over 80 minutes, followed by a washout at

154   80% solvent B for 10 minutes.

155   MS1 spectra were acquired between 300-1750 Thompson at a resolution of 75000 with an AGC

156   target of 3×106 within 250 ms. Using a dynamic exclusion window of 90 sec, the top 10 most

157   intense ions were selected for higher-energy collisional dissociation (HCD) fragmentation with an

158   NCE of 28. MS2 spectra were acquired at a resolution of 17500 and a minimum AGC of 1×103

159   within 80 ms.

160   *Protein and phosphopeptide identification*

161   Raw files were processed in MaxQuant version 1.6.14.0. MS/MS spectra were searched against

162   the *Mus musculus* reference proteome downloaded 7 July 2020 from UniProt

163   (http://www.uniprot.org/proteomes/UP000000589) containing contaminants. Maxquant's built-in

164   Andromeda search algorithm (15) was used to map spectra to the reference proteome with mass

165   tolerance for precursor and fragment ions set at 4.5 ppm and 20 ppm, respectively. The match-

166   between-runs functionality was enabled, by which peptide identifications can be transferred across

167   raw files based on accurate retention time and mass-to-charge ratio (m/z). The identification false-

168   discovery rate (FDR) was estimated using a target-decoy database. Carbamidomethylation of

169   cysteine residues was specified as a fixed modification for all groups. Variable modifications

170   considered were oxidation of methionine and protein N-terminal acetylation for the proteome files,

171   with the addition of phosphorylation of serine, threonine, and tyrosine (Ser/Thr/Tyr) residues for

172   the phosphoproteome files. Trypsin and Lys-C were selected as digestion enzymes and two missed

173   cleavages were allowed.

Statistical processing & bioinformatics analysis

175   The Proteus package (16) in R was used for evidence data exploration, quality checks, and

176   visualisation at the peptide level. Perseus version 1.6.14.0 software (17) was used for quality

177   control, statistical processing, and protein annotation. Protein identifications were filtered for those

178   only identified by site, reverse database hits, and potential contaminants. The log2-transformed

179   protein abundance values were then filtered to contain a minimum of three valid values among the

180   four biological replicates per condition. A two-sample t-test with a Benjamini-Hochberg (BH)

181   FDR threshold of 0.05 was performed to detect differentially abundant proteins.

182   Phosphopeptide identifications were filtered for reverse hits, potential contaminants, and a

183   localisation probability >0.75. The intensity values were log2-transformed before filtering for valid

184   values. The phosphoproteomic intensities were normalised to the proteome intensities by

185   subtraction to account for protein abundance differences and then filtered to contain a minimum

186   of three valid values among the four biological replicates per condition. A median normalisation

187   was also performed across the data set, followed by a two-sample t-test with a BH FDR threshold

188   of 0.05. The identified differentially phosphorylated peptides were functionally annotated and

189   filtered for unique entries.

Functional enrichment and network analysis

191   To identify pathways altered by PknG during mycobacterial infection, we assessed the

192   complement of differentially abundant proteins and phosphoproteins for enriched Kyoto

193   Encyclopaedia of Genes and Genomes (KEGG) pathways using the enrichment analysis tool of

194   the stringApp plug-in within Cytoscape (18, 19) with FDR <0.01. The *Mus musculus* genome was

195 used as the background. Functional enrichment is based on over-representation analysis using

196 hypergeometric tests. Similarly, the complement of differentially phosphorylated proteins and the

197 subset of differentially up-regulated phosphoproteins were used to retrieve enriched Gene

198 Ontology (GO) terms using the stringApp. The enrichment results were filtered for redundancy

199 with a cut-off of 0.25 and GO terms and KEGG pathways identified with less than three proteins

200 were ignored.

201 Visualisation of the functional enrichment networks was performed using the clusterProfiler

202 package (20). Briefly, the genome-wide annotation library (org.Mm.eg.db) for *Mus musculus* was

203 downloaded from Bioconductor (www.bioconductor.org). UniProt IDs of the differentially

204 phosphorylated proteins were converted to Entrez Gene IDs using org.Mm.eg.db as the organism

205 database. We achieved 90.28% mapping rate of our proteins to the annotation database. Gene-

206 concept networks were generated using the GO enrichment analysis results.

207 **Results**

208 *Intracellular survival of mycobacteria in RAW 264.7 macrophages*

209 We monitored the survival dynamics of *M. bovis* BCG WT compared to the ΔPknG mutant, judged

210 by measuring colony-forming units (CFUs) at five-hour intervals post-infection (Figure 1). Our

211 results are in agreement with the work of Walhburger et al. (2004) (9) on which our present study

212 is based. The BCG WT strain displayed a two-fold increase over 24 hours post-infection whilst

213 the null mutant's growth was controlled by the macrophages.

214 *Proteomic analysis of infected RAW 264.7 macrophages with mycobacterial strains*

215 Proteomic experiments were run in parallel to the phosphoproteomic workflow (Figure 2). The

216 evidence data was used to assess the quality of peptide identifications (Figure S1). After initial

217 filtering, the proteomic experiment identified a total of 3441 protein groups. The log2-transformed

218   label-free quantification (LFQ) protein abundance values were then filtered to contain a minimum

219   of three valid values in each group, resulting in 1317 protein groups remaining. After differential

220   analysis, 619 proteins were considered to have significantly different abundance levels between

221   the *M. bovis* WT and ΔPknG samples (Table S1). Of these, 497 host proteins were up-regulated

222   (Table S2).

223   *Identification of PknG-mediated quantitative phosphoproteomic changes in the RAW 264.7*

224   *macrophages during infection*

225   To identify potential host targets of mycobacterial PknG, we employed a label-free quantitative

226   phosphoproteomics approach to study global phosphorylation dynamics associated with PknG

227   during *M. bovis* BCG macrophage infection. Four biological replicates per experiment were

228   analysed to increase the phosphoproteome coverage. We considered proteins phosphorylated in at

229   least three of the four replicates per condition that displayed a statistically significant increase in

230   phosphorylation in the WT as candidate host proteins phosphorylated via the direct or indirect

231   action of PknG.

232   A total of 1401 phosphosites (p-sites) were identified. After removing known contaminants and

233   filtering low-quality data points as previously described, 1371 highly confident phosphopeptides

234   mapped to 914 phosphoproteins were taken for further analysis. The distribution of phosphoserine

235   (pS), phosphothreonine (pT) and phosphotyrosine (pY) sites was 85.3%, 13.4%, and 1.3%,

236   respectively. Moreover, the majority of the peptides were singly phosphorylated (95.1%), whereas

237   approximately 4.9% were multiply phosphorylated. The mass spectrometry proteomics and

238   phosphoproteomics data have been deposited to the ProteomeXchange Consortium

239   (http://proteomecentral.proteomexchange.org) via the PRIDE partner repository with the dataset

240   identifier PXD019365 (21, 22).

241 The quantification of phosphorylated proteins is important to our understanding of the resulting

242 biological effects. To ensure that these differentially regulated phosphopeptides were not because

243 of changes at the proteome level, the phosphoproteomic intensities were normalised to the

244 proteome intensities. The normalised log2-transformed intensities of the RAW 264.7 cells infected

245 with *M. bovis* BCG WT and ΔPknG mutant were then compared using a two-sample t-test with a

246 BH FDR <0.05. A total of 149 peptides were significantly differentially phosphorylated (Table

247 S3). Of these, the 95 p-sites were differentially up-regulated in the presence of mycobacterial PknG

248 (Table S4) with 44 phosphoproteins differentially up-regulated with log2 fold-change (log2FC) >1

249 (Table 1). A volcano plot (Figure 3B) revealed significantly differentially phosphorylated peptides

250 with FDR <0.05. Hierarchical clustering of the differentially up-regulated phosphopeptides with

251 log2FC >1 (Figure 3C) was performed to assess the biological variability between samples. Figure

252 S2 illustrates the relative fractions of pS, pT and pY observed among the differential and non-

253 differential p-site, peptide, and protein identifications.

Functional annotation of host proteins differentially abundant proteins and phosphoproteins in

255 *the presence of PknG*

256 Functional enrichments in our data were retrieved for GO terms and KEGG pathways and filtered

257 for redundancy. A functional enrichment network was built for the significantly differentially

258 abundant proteins and phosphoproteins using the clusterProfiler package (Figure 4). Enriched

259 KEGG pathways of the differentially abundant proteins (Figure 5A) reaffirm PknG's role in the

260 regulation of host metabolism (23) and the phagosome-lysosome interaction (9, 24, 25) to control

261 mycobacterial virulence. These results also propose a role for PknG in the manipulation of host

262 translational, proteasomal, and spliceosomal machinery to promote intracellular survival of the

263 bacilli. Among the functionally enriched KEGG pathways of the differentially phosphorylated

264 proteins (Figure 5B), Fc gamma R-mediated phagocytosis, regulation of actin cytoskeleton, and

265 endocytosis are consistent with previous literature surrounding the intracellular role of

266 mycobacterial PknG during infection (9, 13, 25). However, observing enriched pathways such as

267 RNA transport, the spliceosome, and DNA replication in our dataset suggests that PknG influences

268 a wide range of host cellular processes.

269 Cellular component GO enrichment of the differentially up-regulated phosphoproteins (Figure 6A)

270 shows that the majority of their localisation is in plasma membrane-bounded cell projections, the

271 spliceosomal complex, cytoplasmic region, and actin cytoskeleton. Complementary to this, Figure

272 6B shows that the highly enriched biological processes are mRNA processing, translational

273 initiation, regulation of cellular processes, and actin cytoskeleton organisation. Binding was

274 observed as the most enriched molecular function among the differentially phosphorylated proteins

275 (Figure 6C) and describes molecule interactions which are dominated by cytoskeletal protein

276 binding and nucleic acid binding. Moreover, we see the enrichment of guanyl-nucleotide exchange

277 factor (GEF) activity, which refers to the exchange of guanyl-nucleotides associated with a

278 guanosine triphosphatase (GTPase).

279 Notably, the Rho family GTPases regulate the integrity of the actin cytoskeleton (26). GTPases,

280 RhoA, Rac1, and Cdc42, participate in the regulation of crucial processes that are dependent on

281 the actin cytoskeleton such as cytokinesis, transcriptional activation, phagocytosis, morphology,

282 and migration (27–30). The activation state of Rho GTPases is governed by the balance between

283 the activities of GEFs and GTPase-activating proteins (GAPs) (31). Unsurprisingly, four GAPs

284 and six GEFs were differentially phosphorylated in our data and serve to validate our findings.

285 Following from this, functional enrichment networks of the differentially up-regulated

286 phosphoproteins highlighted subsets of proteins that appear to be interlinked and associated with

287 actin filament organisation, negative regulation of cytoskeleton organisation, response to peptide,

288 regulation of cellular amide metabolism and translational initiation (Figure 7A). Expectedly, the

289 molecular functions that emerge as interlinked include actin binding and SH3 binding, as well as

290 GEF activity and translation regulatory activity (Figure 7B). This highlights mycobacterial PknG's

291 ability to manipulate several key cellular functions during infection of host macrophages.

292 **Discussion**

293 PknG is thought to play an important role in reprogramming macrophage function to aid the

294 survival of tubercle bacilli. Studies have demonstrated that macrophages harbouring *M. bovis* BCG

295 strains failed to induce phagosome maturation, while the mutant lacking PknG was successfully

296 eliminated (9, 32). This prompted us to decipher the host mechanisms exploited by PknG to

297 promote the pathogenesis of TB, by identifying the host proteins phosphorylated by PknG after *M.*

298 *bovis* BCG has been phagocytosed. To this end, we carried out a quantitative label-free

299 phosphoproteomic approach that we, and others, have shown to be a high-throughput platform to

300 identify targets of protein kinases (33–36). The functions of the differentially phosphorylated

301 proteins identified in this study shed new light on the mechanisms that PknG uses to regulate and

302 reprogram host-signalling pathways that enable the bacterium's survival, as discussed below.

303 *PknG mediates the regulation of cytoskeletal organisation*

304 The cytoskeleton is a three-dimensional network of proteins, including actin filaments,

305 microtubules (MTs), and intermediate filaments (IFs) (37, 38). Actin cytoskeletal rearrangement

306 promotes numerous events that are beneficial to intracellular pathogens, including internalisation

307 of bacteria, altered vesicular trafficking, actin-dependent motility, and pathogen dissemination

308 (39). A few groups have explored the role of the actin cytoskeleton during *Mycobacterium* late

309 phases of phagocytosis. Guérin & De Chastellier (2000) showed that *Mycobacterium avium*

310   disrupts the macrophage actin filament network, highlighting the target for the bacterium that

311   allows sustained intracellular survival (40). Anes et al. (2003) demonstrated that in contrast to non-

312   pathogenic mycobacteria, pathogenic *Mtb* prevents actin polymerisation on phagosomal

313   membranes (41). We have identified six phosphoproteins that we believe are indicative of

314   disruptive cytoskeletal remodelling in the presence of PknG.

315   *Rho GTPase-mediated cytoskeletal remodelling* – As previously mentioned, GEFs and GAPs

316   modulate Rho GTPase activity and ultimately coordinate cytoskeleton remodelling (26, 31). GEF-

317   H1 is a unique GEF that associates with microtubules and is known to mediate the crosstalk

318   between MTs and the actin cytoskeleton, which may contribute to the phagocytosis of bacteria by

319   macrophages (42). The activity of GEF-H1 is suppressed when it is bound to the dynein motor

320   complex on MTs (43, 44) and activated when released from MTs upon the intracellular binding of

321   bacterial effectors (45, 46). A recent study showed that the expression of GEF-H1 was increased

322   via the MAPK signalling pathway during mycobacterial infection and silencing of GEF-H1

323   inhibited macrophage-mediated mycobacterial phagocytosis and elimination c

324   Various studies have shown that GEF-H1 is both positively and negatively regulated via

325   phosphorylation. For instance, it has been reported that GEF-H1 phosphorylation in the C-terminal

326   portion on S885 and S959 contributes to holding GEF-H1 in a catalytically inactive configuration,

327   thus inhibiting its GEF activity (47, 48). In contrast, phosphorylation that occurs between the PH

328   and coiled-coil domain of GEF-H1 at S151 and T678 causes dissociation from microtubules (49,

329   50). This is followed by stimulation of RhoA activation, resulting in the formation of focal

330   adhesions and stress fibres, thereby enabling actin cytoskeleton remodelling.

331   We identified phosphorylation of GEF-H1 at S902, which falls within the C-terminal region and

332   should correspond with negative regulation of GEF activity. This suggests that phosphorylation of

333 GEF-H1 in the presence of PknG hinders RhoA activation, thereby contributing to the

334 disruption/uncoupling of actin stress fibres and focal adhesions. Such modification to the

335 organisation and structure of the host cytoskeleton would promote the survival and growth of the

336 bacterium in host macrophages, consistent with the GEF-H1 silencing studies discussed above,

337 consistent with the GEF-H1 silencing studies discussed above (46).

338 The Rac1/Cdc42 GEF, ARHGEF6, plays certain roles in some immune cells, including neutrophils

339 and T cells. Importantly, ARHGEF6 is required for the activation of Ser/Thr-protein kinase PAK

340 2 (PAK2) and subsequent LIM-kinase (LIMK)-dependent inactivation of cofilin. Cofilin-1 (Cfl1)

341 was significantly dephosphorylated in the presence of PknG in our dataset. ARHGEF6 was found

342 to be differentially phosphorylated at S663 and S703 in this study and the phosphorylation of

343 PAK2 at S2 and S55 were significantly up-regulated and down-regulated, respectively.

344 Collectively, the ARHGEF6/Rac1/PAK2/LIMK/cofilin signalling module limits actin turnover by

345 confining both lamellipodial actin polymerisation and depolymerisation, enables polarized, stable

346 lamellipodia formation, and promotes focal complex assembly in lymphocytes (51). Since

347 phosphorylation of Cfl1 suppresses its activity, our study indicates enhanced actin

348 depolymerisation and disruption of actin stress fibres and focal adhesion complexes in the presence

349 of PknG. This also suggests that phosphorylation of ARHGEF6 at S663/703 has an inhibitory

350 effect on its Rac1 GEF activity.

351 Similarly, DOCK2 activates Rac-dependent actin polymerization and contributes to T and B cell

352 migration (52, 53). Dendritic cells defective in DOCK2 exhibit impaired endocytosis of soluble

353 antigens and phagocytosis of insoluble antigens and larger particles (54). Moreover, DOCK10, a

354 Rac1/Cdc42 GEF, is known to affect cell morphology, spreading, and actin cytoskeleton

355   protrusions of adherent HeLa cells (55). Together, phosphorylation of these GEFs reaffirms the

356   role that PknG plays in disrupting cytoskeletal organisation during infection.

357   Furthermore, LIM domain and actin-binding protein 1 (Lima1, also known as EPLIN) is involved

358   in actin cytoskeleton regulation and dynamics. Lima1 cross-links and bundles actin filaments,

359   thereby stabilising actin stress fibres. Lima1 inhibits Arp2/3 complex-mediated branching

360   nucleation of actin filaments, thus controlling actin filament dynamics by stabilising actin filament

361   networks (56). Phosphorylation of the C-terminal region of Lima1 inhibits its actin-binding

362   activity (57). Thus, the increased phosphorylation of Lima1 in the presence of PknG contributes

363   to the reduced stability of actin stress fibres and increased actin filament depolymerisation, as

364   observed with GEF-H1.

365   *PknG inhibits phagosome maturation* – Mammalian nucleoside diphosphate kinase (NDPK)

366   proteins participate in the regulation of multiple cellular processes via enzymatic and non-

367   enzymatic functions. Their primary enzymatic function is to catalyse the conversion of nucleoside

368   diphosphates (NDPs) into nucleoside triphosphates (NTPs) (58). Here, NDPK-A [also known as

369   NME1, NM23-H1/NM23-M1 (human/mouse homolog)] was identified with differential

370   phosphorylation on T94 in the presence of PknG. Mounting evidence suggests that NDPK-A

371   interacts with and affects various components and regulators of the cytoskeleton, including actin-

372   binding proteins, IFs, and cytoskeletal attachment structures (59–66). Garzia et al. (2008)

373   demonstrated that increased phosphorylation of NDPK-A promotes cell motility in breast cancer

374   cells (67). Importantly, NDPK-A possesses GAP activity and negatively regulates Rho-Rac

375   signalling through the inhibition of Rac1 activity (68, 69). NDK-A silencing increased Rac1

376   signalling and MAPK/SAPK (stress-activated protein kinases) activation (60).

377   A recent study showed that NDPK-A is a phagocytosis promoting factor and acts in a complex

378   with Dynamin (DYN-1) on phagosomal surfaces, during engulfment and the early stages of

379   phagosome maturation (66). NDPK-A depletion in macrophages led to decreased phagocytic

380   capacity (66). Furthermore, NDPKs are known to be secreted by mycobacteria, including *Mtb* and

381   *M. bovis* BCG (70, 71). *In vitro* analyses demonstrated that mycobacterial NDPK possesses GAP

382   activity towards Rho GTPases, Rab5 and Rab7, which regulate endosomal trafficking in

383   macrophages. It is suggested that mycobacterial NDPK disrupts the maturation and lysosome

384   fusion of phagosome-containing pathogenic mycobacteria by inactivating Rab5 and Rab7 (72, 73).

385   Similarly, when bacteria are phagocytosed by antigen-presenting cells, the phagosome acquires

386   early endosomal protein markers, such as early endosomal antigen 1 (EEA1) and Rab5, which are

387   gradually replaced with Rab7 during the maturation of the phagosome (74, 75). It has been reported

388   that phagosomes containing live pathogenic mycobacteria do not acquire Rab5 due to the transient

389   recruitment and active retention of coronin-1A (also known as tryptophan aspartate coat protein

390   (TACO) or p57) (76). Hence, stable phagosomal association with coronin-1A results in the

391   inhibition of phagosomal maturation (77).

392   We identified the host F-actin-binding protein coronin-1A to be differentially phosphorylated on

393   T418. Upregulation of T418 was also previously observed during the first 10 minutes after

394   lipopolysaccharide (LPS) and Pam3Cys stimulation of macrophages (78). Notably,

395   phosphorylation of coronin-1A deregulates its association with F-actin, which, in turn, facilitates

396   early phagosome formation (50). Schuller et al. (2001) also found that *Mtb* inhibits lysosome

397   formation by increasing the expression of coronin1-A on the phagosomal membrane (79).

398   Together, our results suggest that PknG phosphorylation of GEFs, GAPs, and actin-binding

399   proteins aids pathogenic mycobacteria to establish its niche within host macrophages through the

400   disruption of actin stress fibres, actin depolymerisation, and inhibition of phagosome maturation.

401   *PknG manipulates host programmed cell death and inflammatory pathways to facilitate*

402   *mycobacterial survival*

403   *Mtb* infection triggers intracellular signalling pathways, enhancing pro-inflammatory responses

404   that are crucial for controlling *Mtb* replication and the immunopathologic response (80). Apoptosis

405   of infected macrophages is associated with diminished pathogen viability (81). However, virulent

406   mycobacteria are known to evade apoptosis which aids the pathogenesis of these strains (82, 83).

407   Apoptotic chromatin condensation inducer in the nucleus (Acin1, also known as acinus) is a

408   multifunctional protein with proposed roles in apoptosis and alternative RNA splicing (84). We

409   identified Acin1 with differentially up-regulated p-sites S937, S656, and S425. Acin1 undergoes

410   several proteolytic cleavages during apoptosis. However, Akt-mediated phosphorylation of Acin1

411   on S422 and S573 residues promotes resistance against proteolytic/apoptotic cleavage in the

412   nucleus and inhibition of acin1-dependent chromatin condensation, thereby facilitating cell

413   survival (85). Interestingly, Banfalvi (2014) identified anomalies in chromatin condensation

414   associated with the apoptosis process in *Mtb*-infected macrophages (86).

415   Acin1 is also an auxiliary component of the exon junction complex (EJC) which is assembled

416   throughout pre-mRNA splicing. The recruitment of a trimeric complex composed of Acin1,

417   SAP18, and RNPS1 to the EJC was reported to modulate apoptotic and splicing regulation.

418   Nevertheless, Acin1 independently regulates splicing profiles of apoptotic genes (87, 88). Our

419   findings, therefore, suggest that PknG plays a role in the inhibition of apoptosis to promote

420   bacterial survival and persistence.

421 Autophagy is known to contribute to the killing of intracellular microbes, including *Mtb*, by

422 modulating host resistance against infections and controlling cellular survival (89–91). Also,

423 autophagy activation aids in regulating inflammation, contributing to a more efficient innate

424 immune response against *Mtb*. *In vitro* studies have shown that mycobacteria escaping from

425 phagosomes into the cytosol are ubiquitinated and targeted by selective autophagy receptors (92,

426 93), such as Sequestosome 1 (SQSTM1; also known as p62).

427 We identified SQSTM1 to be differentially phosphorylated on residues S269 and S27. This

428 signalling adaptor is central to cell survival and proliferation through the activation of the

429 mechanistic target of rapamycin complex 1 (mTORC1). The mechanistic target of rapamycin

430 (mTOR) is a key regulator of autophagy, cell metabolism, growth, proliferation, translation

431 initiation, and cytoskeletal organization. Importantly, autophagy is inhibited by mTORC1

432 activation (94). Phosphorylation of T269 and S272 (T272 in *Mus musculus*) on SQSTM1 seems

433 to be necessary for autophagic inhibition under nutrient-rich conditions (95). Hence, SQSTM1

434 phosphorylation in the presence of PknG plays a role in facilitating mycobacterial survival and

435 proliferation within the host by diminishing autophagy-mediated clearance. Our findings suggest

436 that PknG enhances mycobacterial virulence by phosphorylating and inhibiting components of the

437 intrinsic cell death machinery.

438 Moreover, during impaired autophagy, SQSTM1 accumulates and activates inflammation via

439 nuclear factor kappa B (NF-κB) (96). We identified NF-κB1 subunit p105 to be differentially

440 phosphorylated at S447 in the presence of PknG. NF-κB1 p105 functions both as a precursor of

441 NF-κB1 p50 and as a cytoplasmic inhibitor of NF-κB. The consequence(s) of S447

442 phosphorylation has yet to be explored. However, well-studied p150 p-sites, such as S893, S903,

443 S907, S927, and S932, point to phosphorylation being a key factor in the outcome of proteasomal

444 processing (partial or complete degradation) of p105 (97–99). Importantly, p105 is also a negative

445 regulator of MAPK activation downstream of various receptors, including TLRs and tumour

446 necrosis factor (TNF) receptors (100, 101).

447 The mycobacterial cell wall contains several pro-inflammatory TLR2 ligands and induces

448 activation of the MAPKs and NF-κB pathways (102, 103). The MAPK pathways play an important

449 role in enhancing antimycobacterial activity and the production of pro-inflammatory mediators,

450 including TNF-α (102), which contribute to phagocytosis, intracellular killing, T cell activation,

451 and granuloma formation (104). Wu et al. (2018) demonstrated that overexpression of PknG in

452 macrophages decreased intracellular cytokine levels, thus promoting mycobacterial survival (105).

453 In particular, PknG was shown to inhibit the inflammatory response through suppression of NF-

454 κB and ERK1/2 pathways. Hence, our findings of differential phosphorylation of NF-κB1 p105

455 potentially provide a mechanistic basis for the inhibitory role of PknG in pro-inflammatory

456 cytokine induction.

457 *PknG promotes mycobacterial survival through translational control*

458 Translational regulation of host mRNAs provides direct and rapid alterations in intracellular levels

459 of the encoded proteins, while simultaneously providing reversibility through modifications such

460 as phosphorylation (106). Therefore, cellular adaptation during physiological stress conditions,

461 such as pathogen infection, attenuate general cellular translation by manipulating the activity of

462 the protein synthesis machinery to antagonise the host immune system. Translational control

463 occurs predominately at the initiation phase which is mainly modulated by the activity of several

464 eukaryotic initiation factors (eIFs). We identified a total of 6 eIFs as differentially up-regulated

465 phosphoproteins in our data, namely eIF2B5 (also known as eIF2Bε), eIF3B, eIF4G3, and eIF5B.

466   Since eIF3B and eIF5B are both involved in IRES-dependent translation initiation (107–109), their

467   differential phosphorylation in the presence of PknG supports the existence of non-canonical

468   translation mechanisms that could contribute to the environmental adaptation by pathogenic

469   mycobacteria. For example, under conditions of cellular stress and subsequent eIF2α

470   phosphorylation (inactivation), IRES-dependent translation of X chromosome-linked inhibitor of

471   apoptosis protein (XIAP) mRNA relies on eIF5B (107). Notably, the XIAP is associated with cell

472   survival by protecting cells from caspase-mediated apoptosis (22–25). Additionally, the eIF4G3

473   protein is a central player in the initiation of translation since it also contains binding domains for

474   mRNA, eIF4A, and eIF3. Many viruses have been shown to interfere with the function of the

475   eIF4F complex to gain control of translation. Some viruses cleave eIF4G3 to arrest host protein

476   translation (110) while other viruses co-opt eIF4G3 to generate viral proteins (111). Overall, the

477   differential phosphorylation of several eIFs in our data suggests that PknG confers substantial

478   control on protein translation and turnover in host cells, potentially preventing the activation of

479   antimycobacterial responses.

480   *PknG contributes to the regulation of alternative mRNA splicing*

481   Alternative splicing of transcripts brings unprecedented diversity to the eukaryotic proteome that

482   can alter protein stoichiometry and physiological consequences (112). Recent studies suggest that

483   the co-option and hijacking of host splicing machinery by pathogens contributes to the perturbation

484   of the host immune response during infection (113, 114). Findings by Kalam et al. (2017) strongly

485   indicated that infection with *Mtb* alters the global patterns of alternate splicing within macrophages

486   (114). Several host splicing factors having been previously identified as interacting partners for

487   various mycobacterial proteins (115, 116). Comparably, we identified a subset of interacting host

488   spliceosomal proteins to be differentially phosphorylated in the presence of PknG, including

489   U4/U6 small nuclear ribonucleoprotein Prp3 (PRP3), heterogeneous nuclear ribonucleoprotein A1

490   (hnRNP-A1), THO complex subunit 4 (THOC4), and U1 small nuclear ribonucleoprotein 70 kDa

491   (snRNP70). Differential levels of these phosphoproteins in our data suggest that PknG promotes

492   aberrant interactions within the host splicing machinery to interfere with the ability of the

493   macrophage to kill the mycobacterium.

494   Moreover, the co-transcriptional RNA processing enzyme, 5′-3′ exoribonuclease 2 (XRN2) was

495   differentially phosphorylated on residues S499 and S501 in the presence of PknG. XRN2 plays a

496   major role in ribosomal RNA (rRNA) maturation, gene silencing (117–120), and DNA damage

497   response and replication stress (121). Cells deficient in XRN2 displayed increased double-strand

498   breaks (DSBs) and genomic instability, along with decreased DNA repair capacity (121).

499   Interestingly, Castro-Garza et al. (2018) demonstrated that *Mtb* infection promoted genomic

500   instability in macrophages through the observation of several DNA damage markers (122).

501   Another study showed that *Mtb* induced DSBs, compared to single-stranded DNA generation

502   initiated by the avirulent strain (123), which provided a survival niche through activation of the

503   ATM-Akt signalling cascade that results in the inhibition of apoptosis and accentuation of cell

504   growth.

505   **Conclusion**

506   In this study, we have employed label-free mass-spectrometry based phosphoproteomics to unravel

507   the mechanisms that pathogenic mycobacteria use – particularly, those mediated by PknG – to

508   evade host immune responses and survive during the early stages of infection. Our data revealed

509   the multifactorial signalling pathways exploited by PknG to promote mycobacterial survival in

510   host macrophages, including perturbation of host actin cytoskeleton organisation and phagosome

511   maturation, inhibition of apoptotic pathways and NF-kB-mediated inflammatory responses,

512   impairment of autophagy, as well as manipulation of alternative splicing, translation and of DNA

513   repair processes. In each case, we find supporting data in the literature validating these

514   perturbations, but importantly our phosphoproteomic data provides significant new mechanistic

515   detail on PknG-mediated post-translational control of these host processes.

516   This work, therefore, considerably increases our current knowledge of mycobacterial

517   pathogenicity and may additionally identify novel molecular approaches to effectively reactivate

518   particular host cellular pathways to restore macrophage capability of mycobacterial elimination.

519   However, to confidently classify these proteins as direct or indirect host substrates of PknG,

520   validation studies are necessary. Validation through targeted parallel reaction monitoring (PRMs)

521   MS assays and imaging experiments are now underway and will be reported elsewhere.

Acknowledgements

References

1. World Health Organization. 2020. Global tuberculosis report 2020: executive summary.

2. Houben RMGJ, Dodd PJ. 2016. The Global Burden of Latent Tuberculosis Infection: A Re-estimation Using Mathematical Modelling. PLoS Med 13:e1002152.

3. Kiazyk S, Ball T. 2017. Latent tuberculosis infection: An overview. Canada Commun Dis Rep 43:62–66.

4. Zhai W, Wu F, Zhang Y, Fu Y, Liu Z. 2019. The immune escape mechanisms of Mycobacterium Tuberculosis. Int J Mol Sci 20:340.

5. Koul A, Herget T, Klebl B, Ullrich A. 2004. Interplay between mycobacteria and host signalling pathways. Nat Rev Microbiol 2:189–202.

6. Mitchell G, Chen C, Portnoy DA. 2016. Strategies Used by Bacteria to Grow in Macrophages, p. 701–725. *In* Myeloid Cells in Health and Disease. American Society of Microbiology.

7. Margenat M, Labandera AM, Gil M, Carrion F, Purificação M, Razzera G, Portela MM, Obal G, Terenzi H, Pritsch O, Durán R, Ferreira AM, Villarino A. 2015. New potential eukaryotic substrates of the mycobacterial protein tyrosine phosphatase PtpA: Hints of a bacterial modulation of macrophage bioenergetics state. Sci Rep 5:1–11.

8. Wehenkel A, Bellinzoni M, Graña M, Duran R, Villarino A, Fernandez P, Andre-Leroux G, England P, Takiff H, Cerveñansky C, Cole ST, Alzari PM. 2008. Mycobacterial Ser/Thr protein kinases and phosphatases: Physiological roles and therapeutic potential. Biochim Biophys Acta - Proteins Proteomics 1784:193–202.

9. Walburger A, Koul A, Ferrari G, Nguyen L, Prescianotto-Baschong C, Huygen K, Klebl B, Thompson C, Bacher G, Pieters J. 2004. Protein kinase G from pathogenic mycobacteria

555   promotes survival within macrophages. Science (80-) 304:1800–1804.

556   10.   Bach H, Papavinasasundaram KG, Wong D, Hmama Z, Av-Gay Y. 2008. Mycobacterium

557   tuberculosis Virulence Is Mediated by PtpA Dephosphorylation of Human Vacuolar Protein

558   Sorting 33B. Cell Host Microbe 3:316–322.

559   11.   Chao J, Wong D, Zheng X, Poirier V, Bach H, Hmama Z, Av-Gay Y. 2010. Protein kinase

560   and phosphatase signaling in Mycobacterium tuberculosis physiology and pathogenesis.

561   Biochim Biophys Acta - Proteins Proteomics 1804:620–627.

562   12.   Sharma AK, Arora D, Singh LK, Gangwal A, Sajid A, Molle V, Singh Y, Nandicoori VK.

563   2016. Serine/threonine protein phosphatase pstp of mycobacterium tuberculosis is

564   necessary for accurate cell division and survival of pathogen. J Biol Chem 291:24215–

565   24230.

566   13.   Scherr N, Müller P, Perisa D, Combaluzier B, Jenö P, Pieters J. 2009. Survival of pathogenic

567   mycobacteria in macrophages is mediated through autophosphorylation of protein kinase G.

568   J Bacteriol 191:4546–4554.

569   14.   Nakedi KC, Calder B, Banerjee M, Giddey A, Nel AJM, Garnett S, Blackburn JM, Soares

570   NC. 2018. Identification of novel physiological substrates of mycobacterium bovis BCG

571   protein Kinase G (PknG) by label-free quantitative phosphoproteomics. Mol Cell

572   Proteomics 17:1365–1377.

573   15.   Cox J, Neuhauser N, Michalski A, Scheltema RA, Olsen J V., Mann M. 2011. Andromeda:

574   A peptide search engine integrated into the MaxQuant environment. J Proteome Res

575   10:1794–1805.

576   16.   Gierlinski M, Gastaldello F, Cole C, Barton GJ. 2018. Proteus: An R package for

577   downstream analysis of MaxQuant output. bioRxiv https://doi.org/10.1101/416511.

578   17.   Tyanova S, Temu T, Sinitcyn P, Carlson A, Hein MY, Geiger T, Mann M, Cox J. 2016. The

579   Perseus computational platform for comprehensive analysis of (prote)omics data. Nat

580   Methods 13:731–740.

581 18. Doncheva NT, Morris JH, Gorodkin J, Jensen LJ. 2019. Cytoscape StringApp: Network

582   Analysis and Visualization of Proteomics Data. J Proteome Res 18:623–632.

583 19. Smoot ME, Ono K, Ruscheinski J, Wang PL, Ideker T. 2011. Cytoscape 2.8: New features

584   for   data   integration   and   network   visualization.   Bioinformatics

585   https://doi.org/10.1093/bioinformatics/btq675.

586 20. Yu G, Wang LG, Han Y, He QY. 2012. ClusterProfiler: An R package for comparing

587   biological themes among gene clusters. Omi A J Integr Biol 16:284–287.

588 21. Deutsch EW, Csordas A, Sun Z, Jarnuczak A, Perez-Riverol Y, Ternent T, Campbell DS,

589   Bernal-Llinares M, Okuda S, Kawano S, Moritz RL, Carver JJ, Wang M, Ishihama Y,

590   Bandeira N, Hermjakob H, Vizcaíno JA. 2017. The ProteomeXchange consortium in 2017:

591   Supporting the cultural change in proteomics public data deposition. Nucleic Acids Res

592   gkw936.

593 22. Perez-Riverol Y, Csordas A, Bai J, Bernal-Llinares M, Hewapathirana S, Kundu DJ,

594   Inuganti A, Griss J, Mayer G, Eisenacher M, Pérez E, Uszkoreit J, Pfeuffer J, Sachsenberg

595   T, Yilmaz Ş, Tiwary S, Cox J, Audain E, Walzer M, Jarnuczak AF, Ternent T, Brazma A,

596   Vizcaíno JA. 2019. The PRIDE database and related tools and resources in 2019: Improving

597   support for quantification data. Nucleic Acids Res D442–D450.

598 23. Rieck B, Degiacomi G, Zimmermann M, Cascioferro A, Boldrin F, Lazar-Adler NR, Bottrill

599   AR, le Chevalier F, Frigui W, Bellinzoni M, Lisa MN, Alzari PM, Nguyen L, Brosch R,

600   Sauer U, Manganelli R, O'Hare HM. 2017. PknG senses amino acid availability to control

601   metabolism and virulence of Mycobacterium tuberculosis. PLoS Pathog 13:e1006399.

602 24. Scherr N, Müller P, Perisa D, Combaluzier B, Jenö P, Pieters J. 2009. Survival of pathogenic

603   mycobacteria in macrophages is mediated through autophosphorylation of protein kinase G.

604   J Bacteriol 191:4546–4554.

605   25.   Pradhan G, Shrivastva R, Mukhopadhyay S. 2018. Mycobacterial PknG Targets the Rab7l1

606   Signaling Pathway To Inhibit Phagosome–Lysosome Fusion. J Immunol 201:1421–1433.

607   26.   Hall A. 1998. Rho GTpases and the actin cytoskeleton. Science (80-) 279:509–514.

608   27.   Aspenström P. 1999. The Rho GTPases have multiple effects on the actin cytoskeleton. Exp

609   Cell Res 246:20–25.

610   28.   Aspenström P. 1999. Effecters for the Rho GTPases. Curr Opin Cell Biol 11:95–102.

611   29.   Jaffe AB, Hall A. 2005. Rho GTPases: Biochemistry and biology. Annu Rev Cell Dev Biol.

612   30.   Aguilera M, Salinas R, Rosales E, Carminati S, Colombo MI, Berón W. 2009. Actin

613   dynamics and Rho GTPases regulate the size and formation of parasitophorous vacuoles

614   containing Coxiella burnetii. Infect Immun 77:4609–4620.

615   31.   Schmidt A, Hall A. 2002. Guanine nucleotide exchange factors for Rho GTPases: Turning

616   on the switch. Genes Dev 16:1587–1609.

617   32.   Sundaramurthy V, Korf H, Singla A, Scherr N, Nguyen L, Ferrari G, Landmann R, Huygen

618   K, Pieters J. 2017. Survival of Mycobacterium tuberculosis and Mycobacterium bovis BCG

619   in lysosomes in vivo. Microbes Infect 19:515–526.

620   33.   Nakedi KC, Calder B, Banerjee M, Giddey A, Nel AJM, Garnett S, Blackburn JM, Soares

621   NC. 2018. Identification of Novel Physiological Substrates of Mycobacterium bovis BCG

622   Protein Kinase G (PknG) by Label-free Quantitative Phosphoproteomics. Mol Cell

623   Proteomics 17:1365–1377.

624   34.   Baros SS, Blackburn JM, Soares NC. 2020. Phosphoproteomic approaches to discover

625   novel substrates of mycobacterial Ser/Thr protein kinases. Mol Cell Proteomics 19:233–

626   244.

627   35.   Gil M, Lima A, Rivera B, Rossello J, Urdániz E, Cascioferro A, Carrión F, Wehenkel A,

628   Bellinzoni M, Batthyány C, Pritsch O, Denicola A, Alvarez MN, Carvalho PC, Lisa MN,

629   Brosch R, Piuri M, Alzari PM, Durán R. 2019. New substrates and interactors of the

630   mycobacterial Serine/Threonine protein kinase PknG identified by a tailored interactomic

631   approach. J Proteomics 192:321–333.

632   36.   Turapov O, Forti F, Kadhim B, Ghisotti D, Sassine J, Straatman-Iwanowska A, Bottrill AR,

633   Moynihan PJ, Wallis R, Barthe P, Cohen-Gonsaud M, Ajuh P, Vollmer W, Mukamolova G

634   V. 2018. Two Faces of CwlM, an Essential PknB Substrate, in Mycobacterium tuberculosis.

635   Cell Rep 25:57-67.e5.

636   37.   Ciobanasu C, Faivre B, Le Clainche C. 2013. Integrating actin dynamics,

637   mechanotransduction and integrin activation: The multiple functions of actin binding

638   proteins in focal adhesions. Eur J Cell Biol 92:339–348.

639   38.   Popowicz GM, Schleicher M, Noegel AA, Holak TA. 2006. Filamins: promiscuous

640   organizers of the cytoskeleton. Trends Biochem Sci 31:411–419.

641   39.   Colonne PM, Winchell CG, Voth DE. 2016. Hijacking host cell highways: Manipulation of

642   the host actin cytoskeleton by obligate intracellular bacterial pathogens. Front Cell Infect

643   Microbiol 6:107.

644   40.   Guérin I, De Chastellier C. 2000. Pathogenic mycobacteria disrupt the macrophage actin

645   filament network. Infect Immun 68:2655–2662.

646   41.   Anes E, Kühnel MP, Bos E, Moniz-Pereira J, Habermann A, Griffiths G. 2003. Selected

647   lipids activate phagosome actin assembly and maturation resulting in killing of pathogenic

648   mycobacteria. Nat Cell Biol 5:793–802.

649   42.   Wang H, Wang J, Yang J, Yang X, He J, Wang R, Liu S, Zhou L, Ma L. 2017. Guanine

650   nucleotide exchange factor -H1 promotes inflammatory cytokine production and

651   intracellular mycobacterial elimination in macrophages. Cell Cycle 16:1695–1704.

652   43.   Chiang H Sen, Zhao Y, Song JH, Liu S, Wang N, Terhorst C, Sharpe AH, Basavappa M,

653   Jeffrey KL, Reinecker HC. 2014. GEF-H1 controls microtubule-dependent sensing of

654   nucleic acids for antiviral host defenses. Nat Immunol 5:63–71.

655   44.   Meiri D, Marshall CB, Greeve MA, Kim B, Balan M, Suarez F, Wu C, LaRose J, Fine N,

656   Ikura M, Rottapel R. 2012. Mechanistic Insight into the Microtubule and Actin

657   Cytoskeleton Coupling through Dynein-Dependent RhoGEF Inhibition. Mol Cell 45:642–

658   655.

659   45.   Fukazawa A, Alonso C, Kurachi K, Gupta S, Lesser CF, McCormick BA, Reinecker HC.

660   2008. GEF-H1 mediated control of NOD1 dependent NF-κB activation by Shigella

661   effectors. PLoS Pathog 4:e1000228.

662   46.   Matsuzawa T, Kuwae A, Yoshida S, Sasakawa C, Abe A. 2004. Enteropathogenic

663   Escherichia coli activates the RhoA signaling pathway via the stimulation of GEF-H1.

664   EMBO J 23:3570–3582.

665   47.   Zenke FT, Krendel M, DerMardirossian C, King CC, Bohl BP, Bokoch GM. 2004. p21-

666   activated Kinase 1 Phosphorylates and Regulates 14-3-3 Binding to GEF-H1, a

667   Microtubule-localized Rho Exchange Factor. J Biol Chem 279:18392–18400.

668   48.   Yamahashi Y, Saito Y, Murata-Kamiya N, Hatakeyama M. 2011. Polarity-regulating kinase

669   partitioning-defective 1b (PAR1b) phosphorylates guanine nucleotide exchange factor H1

670   (GEF-H1) to regulate RhoA-dependent actin cytoskeletal reorganization. J Biol Chem

671   286:44576–44584.

672   49.   Sandi MJ, Marshall CB, Balan M, Coyaud E, Zhou M, Monson DM, Ishiyama N,

673   Chandrakumar AA, La Rose J, Couzens AL, Gingras AC, Raught B, Xu W, Ikura M,

674   Morrison DK, Rottapel R. 2017. MARK3-mediated phosphorylation of ARHGEF2 couples

675 microtubules to the actin cytoskeleton to establish cell polarity. Sci Signal 10:eaan3286.

676 50. Fujishiro S hei, Tanimura S, Mure S, Kashimoto Y, Watanabe K, Kohno M. 2008. ERK1/2

677 phosphorylate GEF-H1 to enhance its guanine nucleotide exchange activity toward RhoA.

678 Biochem Biophys Res Commun 368:162–167.

679 51. Mamula D. 2019. ARHGEF6 controls speed and directionality of lymphocyte migration by

680 regulating Rac1PAK2/LIMK1/cofilion signaling pathway. Otto-von-Guericke-Universität

681 Magdeburg.

682 52. Nombela-Arrieta C, Mempel TR, Soriano SF, Mazo I, Wymann MP, Hirsch E, Martínez-

683 A. C, Fukui Y, Von Andrian UH, Stein J V. 2007. A central role for DOCK2 during

684 interstitial lymphocyte motility and sphingosine-1-phosphate-mediated egress. J Exp Med

685 204:497–510.

686 53. Fukui Y, Hashimoto O, Sanui T, Oono T, Koga H, Abe M, Inayoshi A, Noda M, Oike M,

687 Shirai T, Sasazuki T. 2001. Haematopoietic cell-specific CDM family protein DOCK2 is

688 essential for lymphocyte migration. Nature 412:826–831.

689 54. Ippagunta SK, Malireddi RKS, Shaw PJ, Neale GA, Walle L Vande, Green DR, Fukui Y,

690 Lamkanfi M, Kanneganti TD. 2011. The inflammasome adaptor ASC regulates the function

691 of adaptive immune cells by controlling Dock2-mediated Rac activation and actin

692 polymerization. Nat Immunol 12:1010–1016.

693 55. Ruiz-Lafuente N, Alcaraz-García MJ, García-Serna AM, Sebastián-Ruiz S, Moya-Quiles

694 MR, García-Alonso AM, Parrado A. 2015. Dock10, a Cdc42 and Rac1 GEF, induces loss

695 of elongation, filopodia, and ruffles in cervical cancer epithelial HeLa cells. Biol Open

696 4:627–635.

697 56. Maul RS, Song Y, Amann KJ, Gerbin SC, Pollard TD, Chang DD. 2003. EPLIN regulates

698 actin dynamics by cross-linking and stabilizing filaments. J Cell Biol 160:399–407.

699   57.   Han M-Y, Kosako H, Watanabe T, Hattori S. 2007. Extracellular Signal-Regulated

700   Kinase/Mitogen-Activated Protein Kinase Regulates Actin Organization and Cell Motility

701   by Phosphorylating the Actin Cross-Linking Protein EPLIN. Mol Cell Biol 27:8190–8204.

702   58.   Lu Z, Hunter T. 2018. Metabolic Kinases Moonlighting as Protein Kinases. Trends Biochem

703   Sci 43:301–310.

704   59.   Conery AR, Sever S, Harlow E. 2010. Nucleoside diphosphate kinase Nm23-H1 regulates

705   chromosomal stability by activating the GTPase dynamin during cytokinesis. Proc Natl

706   Acad Sci U S A 107:15461–15466.

707   60.   Boissan M, De Wever O, Lizarraga F, Wendum D, Poincloux R, Chignard N, Desbois-

708   Mouthon C, Dufour S, Nawrocki-Raby B, Birembaut P, Bracke M, Chavrier P, Gespach C,

709   Lacombe ML. 2010. Implication of metastasis suppressor NM23-H1 in maintaining

710   adherens junctions and limiting the invasive potential of human cancer cells. Cancer Res

711   70:7710–7722.

712   61.   Boissan M, Montagnac G, Shen Q, Griparic L, Guitton J, Romao M, Sauvonnet N, Lagache

713   T, Lascu I, Raposo G, Desbourdes C, Schlattner U, Lacombe ML, Polo S, Van Der Bliek

714   AM, Roux A, Chavrier P. 2014. Nucleoside diphosphate kinases fuel dynamin superfamily

715   proteins with GTP for membrane remodeling. Science (80-) 344:1510–1515.

716   62.   Marino N, Marshall JC, Collins JW, Zhou M, Qian Y, Veenstra T, Steeg PS. 2013. Nm23-

717   H1 binds to Gelsolin and inactivates its actin-severing capacity to promote tumor cell

718   motility and metastasis. Cancer Res 73:5949–5962.

719   63.   Snider NT, Weerasinghe SVW, Singla A, Leonard JM, Hanada S, Andrews PC, Lok AS,

720   Omary MB. 2011. Energy determinants GAPDH and NDPK act as genetic modifiers for

721   hepatocyte inclusion formation. J Cell Biol 195:217–229.

722   64.   Lombardi D, Sacchi A, D'agostino G, Tibursi G. 1995. The association of the Nm23-M1

723   protein and β-tubulin correlates with cell differentiation. Exp Cell Res 217:267–271.

724 65. Aktary Z, Chapman K, Lam L, Lo A, Ji C, Graham K, Cook L, Li L, MacKey JR, Pasdar

725   M. 2010. Plakoglobin interacts with and increases the protein levels of metastasis suppressor

726   Nm23-H2 and regulates the expression of Nm23-H1. Oncogene 29:2118–2129.

727 66. Farkas Z, Petric M, Liu X, Herit F, Rajnavölgyi É, Szondy Z, Budai Z, Orbán TI, Sándor S,

728   Mehta A, Bajtay Z, Kovács T, Jung SY, Shakir MA, Qin J, Zhou Z, Niedergang F, Boissan

729   M, Takács-Vellai K. 2019. The nucleoside diphosphate kinase NDK-1/NME1 promotes

730   phagocytosis in concert with DYN-1/Dynamin. FASEB J 33:11606–11614.

731 67. Garzia L, D'Angelo A, Amoresano A, Knauer SK, Cirulli C, Campanella C, Stauber RH,

732   Steegborn C, Iolascon A, Zollo M. 2008. Phosphorylation of nm23-H1 by CKI induces its

733   complex formation with h-prune and promotes cell motility. Oncogene 27:1853–1864.

734 68. Otsuki Y, Tanaka M, Yoshii S, Kawazoe N, Nakaya K, Sugimura H. 2001. Tumor

735   metastasis suppressor nm23H1 regulates Rac1 GTPase by interaction with Tiam1. Proc Natl

736   Acad Sci U S A 98:4385–4390.

737 69. Murakami M, Meneses PI, Knight JS, Lan K, Kaul R, Verma SC, Robertson ES. 2008.

738   Nm23-H1 modulates the activity of the guanine exchange factor Dbl-1. Int J Cancer

739   123:500–510.

740 70. Målen H, Berven FS, Fladmark KE, Wiker HG. 2007. Comprehensive analysis of exported

741   proteins from Mycobacterium tuberculosis H37Rv, p. 1702–1718. *In* Proteomics. John

742   Wiley & Sons, Ltd.

743 71. Chopra P, Singh A, Koul A, Ramachandran S, Drlica K, Tyagi AK, Singh Y. 2003.

744   Cytotoxic activity of nucleoside diphosphate kinase secreted from Mycobacterium

745   tuberculosis. Eur J Biochem 270:625–634.

746 72. Sun J, Wang X, Lau A, Liao TYA, Bucci C, Hmama Z. 2010. Mycobacterial nucleoside

747   diphosphate kinase blocks phagosome maturation in murine raw 264.7 macrophages. PLoS

748   One 5:e8769.

749   73.   Chopra P, Koduri H, Singh R, Koul A, Ghildiyal M, Sharma K, Tyagi AK, Singh Y. 2004.

750   Nucleoside diphosphate kinase of Mycobacterium tuberculosis acts as GTPase-activating

751   protein for Rho-GTPases. FEBS Lett 571:212–216.

752   74.   Via LE, Deretic D, Ulmer RJ, Hibler NS, Huber LA, Deretic V. 1997. Arrest of

753   mycobacterial phagosome maturation is caused by a block in vesicle fusion between stages

754   controlled by rab5 and rab7. J Biol Chem 272:13326–13331.

755   75.   Fratti RA, Backer JM, Gruenberg J, Corvera S, Deretic V. 2001. Role of

756   phosphatidylinositol 3-kinase and Rab5 effectors in phagosomal biogenesis and

757   mycobacterial phagosome maturation arrest. J Cell Biol 154:631–644.

758   76.   Ferrari G, Langen H, Naito M, Pieters J. 1999. A coat protein on phagosomes involved in

759   the intracellular survival of mycobacteria. Cell 97:435–447.

760   77.   Pieters J, Gatfield J. 2002. Hijacking the host: Survival of pathogenic mycobacteria inside

761   macrophages. Trends Microbiol 10:142–146.

762   78.   Sjoelund V, Smelkinson M, Nita-Lazar A. 2014. Phosphoproteome profiling of the

763   macrophage response to different toll-like receptor ligands identifies differences in global

764   phosphorylation dynamics. J Proteome Res 13:5185–5197.

765   79.   Schuller S, Neefjes J, Ottenhoff T, Thole J, Young D. 2001. Coronin is involved in uptake

766   of Mycobacterium bovis BCG in human macrophages but not in phagosome maintenance.

767   Cell Microbiol 3:785–793.

768   80.   Cooper AM. 2009. Cell-mediated immune responses in tuberculosis. Annu Rev Immunol

769   27:393–422.

770   81.   Fratazzi C, Arbeit RD, Carini C, Balcewicz-Sablinska MK, Keane J, Kornfeld H, Remold

771   HG. 1999. Macrophage apoptosis in mycobacterial infections, p. 763–764. *In* Journal of

772   Leukocyte Biology. Federation of American Societies for Experimental Biology.

773 82. Keane J, Remold HG, Kornfeld H. 2000. Virulent Mycobacterium tuberculosis Strains

774   Evade Apoptosis of Infected Alveolar Macrophages. J Immunol 164:2016–2020.

775 83. Balcewicz-Sablinska MK, Keane J, Kornfeld H, Remold HG. 1998. Pathogenic

776   Mycobacterium tuberculosis evades apoptosis of host macrophages by release of TNF-R2,

777   resulting in inactivation of TNF-alpha. J Immunol 161:2636–2641.

778 84. Nandi N, Krämer H. 2018. Cdk5-mediated Acn/Acinus phosphorylation regulates basal

779   autophagy independently of metabolic stress. Autophagy 14:1271–1272.

780 85. Hu Y, Yao J, Liu Z, Liu X, Fu H, Ye K. 2005. Akt phosphorylates acinus and inhibits its

781   proteolytic cleavage, preventing chromatin condensation. EMBO J 24:3543–3554.

782 86. Banfalvi G. 2014. Apoptotic agents inducing genotoxicity-specific chromatin changes.

783   Apoptosis 19:1301–1316.

784 87. Michelle L, Cloutier A, Toutant J, Shkreta L, Thibault P, Durand M, Garneau D, Gendron

785   D, Lapointe E, Couture S, Le Hir H, Klinck R, Elela SA, Prinos P, Chabot B. 2012. Proteins

786   Associated with the Exon Junction Complex Also Control the Alternative Splicing of

787   Apoptotic Regulators. Mol Cell Biol 32:954–967.

788 88. Wang F, Soprano KJ, Soprano DR. 2015. Role of acinus in regulating retinoic acid-

789   responsive gene Pre-mRNA splicing. J Cell Physiol 230:791–801.

790 89. Ponpuak M, Davis AS, Roberts EA, Delgado MA, Dinkins C, Zhao Z, Virgin HW, Kyei

791   GB, Johansen T, Vergne I, Deretic V. 2010. Delivery of Cytosolic Components by

792   Autophagic Adaptor Protein p62 Endows Autophagosomes with Unique Antimicrobial

793   Properties. Immunity 32:329–341.

794 90. Bento CF, Empadinhas N, Mendes V. 2015. Autophagy in the fight against tuberculosis.

795   DNA Cell Biol 34:228–242.

796   91.   Bah A, Vergne I. 2017. Macrophage autophagy and bacterial infections. Front Immunol

797   8:1483.

798   92.   Watson RO, Manzanillo PS, Cox JS. 2012. Extracellular M. tuberculosis DNA targets

799   bacteria for autophagy by activating the host DNA-sensing pathway. Cell 150:803–815.

800   93.   Manzanillo PS, Ayres JS, Watson RO, Collins AC, Souza G, Rae CS, Schneider DS,

801   Nakamura K, Shiloh MU, Cox JS. 2013. The ubiquitin ligase parkin mediates resistance to

802   intracellular pathogens. Nature 501:512–516.

803   94.   Jung CH, Ro SH, Cao J, Otto NM, Kim DH. 2010. MTOR regulation of autophagy. FEBS

804   Lett 584:1287–1295.

805   95.   Linares JF, Duran A, Reina-Campos M, Aza-Blanc P, Campos A, Moscat J, Diaz-Meco

806   MT. 2015. Amino Acid Activation of mTORC1 by a PB1-Domain-Driven Kinase Complex

807   Cascade. Cell Rep 12:1339–1352.

808   96.   Takeda-Watanabe A, Kitada M, Kanasaki K, Koya D. 2012. SIRT1 inactivation induces

809   inflammation through the dysregulation of autophagy in human THP-1 cells. Biochem

810   Biophys Res Commun 427:191–196.

811   97.   Fujimoto K, Yasuda H, Sato Y, Yamamoto K ichi. 1995. A role for phosphorylation in the

812   proteolytic processing of the human NF-KB1 precursor. Gene 165:183–189.

813   98.   Lang V, Janzen J, Fischer GZ, Soneji Y, Beinke S, Salmeron A, Allen H, Hay RT, Ben-

814   Neriah Y, Ley SC. 2003. βTrCP-Mediated Proteolysis of NF-κB1 p105 Requires

815   Phosphorylation of p105 Serines 927 and 932. Mol Cell Biol 23:402–413.

816   99.   Cohen S, Achbert-Weiner H, Ciechanover A. 2004. Dual Effects of IκB Kinase β-Mediated

817   Phosphorylation on p105 Fate: SCFβ-TrCP-Dependent Degradation and SCFβ-TrCP-

818   Independent Processing. Mol Cell Biol 24:475–486.

819   100.   Belich MP, Salmerón A, Johnston LH, Ley SC. 1999. TPL-2 kinase regulates the proteolysis
820   of the NF-κb-inhibitory protein NF-κB1 p105. Nature 397:363–368.

821   101.   Beinke S, Deka J, Lang V, Belich MP, Walker PA, Howell S, Smerdon SJ, Gamblin SJ,
822   Ley SC. 2003. NF-κB1 p105 Negatively Regulates TPL-2 MEK Kinase Activity. Mol Cell
823   Biol 23:4739–4752.

824   102.   Jo EK, Yang CS, Choi CH, Harding C V. 2007. Intracellular signalling cascades regulating
825   innate immune responses to Mycobacteria: Branching out from Toll-like receptors. Cell
826   Microbiol 9:1087–1098.

827   103.   Brightbill HD, Libraty DH, Krutzik SR, Yang RB, Belisle JT, Bleharski JR, Maitland M,
828   Norgard M V., Plevy SE, Smale ST, Brennan PJ, Bloom BR, Godowski PJ, Modlin RL.
829   1999. Host defense mechanisms triggered by microbial lipoproteins through toll-like
830   receptors. Science (80-) 285:732–736.

831   104.   Bermudez LEM, Young LS. 1988. Tumor necrosis factor, alone or in combination with IL-
832   2, but not IFN-γ, is associated with macrophage killing of Mycobacterium avium complex.
833   J Immunol 140:3006–3013.

834   105.   Wu FL, Liu Y, Zhang HN, Jiang HW, Cheng L, Guo SJ, Deng JY, Bi LJ, Zhang XE, Gao
835   HF, Tao SC. 2018. Global Profiling of PknG Interactions Using a Human Proteome
836   Microarray Reveals Novel Connections with CypA. Proteomics 18:e1800265.

837   106.   Mazumder B, Li X, Barik S. 2010. Translation Control: A Multifaceted Regulator of
838   Inflammatory Response. J Immunol 184:3311–3319.

839   107.   Thakor N, Holcik M. 2012. IRES-mediated translation of cellular messenger RNA operates
840   in eIF2α-independent manner during stress. Nucleic Acids Res 40:541–552.

841   108.   Masutani M, Sonenberg N, Yokoyama S, Imataka H. 2007. Reconstitution reveals the
842   functional core of mammalian eIF3. EMBO J 26:3373–3383.

843   109.   Fitzgerald KD, Semler BL. 2009. Bridging IRES elements in mRNAs to the eukaryotic

844   translation apparatus. Biochim Biophys Acta - Gene Regul Mech 1789:518–528.

845   110.   Svitkin Y V., Gradi A, Imataka H, Morino S, Sonenberg N. 1999. Eukaryotic Initiation

846   Factor 4GII (eIF4GII), but Not eIF4GI, Cleavage Correlates with Inhibition of Host Cell

847   Protein Synthesis after Human Rhinovirus Infection. J Virol 73:3467–3472.

848   111.   Walsh D. 2010. Manipulation of the host translation initiation complex eIF4F by DNA

849   viruses, p. 1511–1516. *In* Biochemical Society Transactions. Portland Press.

850   112.   Nilsen TW, Graveley BR. 2010. Expansion of the eukaryotic proteome by alternative

851   splicing. Nature 463:457–463.

852   113.   De Maio FA, Risso G, Iglesias NG, Shah P, Pozzi B, Gebhard LG, Mammi P, Mancini E,

853   Yanovsky MJ, Andino R, Krogan N, Srebrow A, Gamarnik A V. 2016. The Dengue Virus

854   NS5 Protein Intrudes in the Cellular Spliceosome and Modulates Splicing. PLoS Pathog

855   12:e1005841.

856   114.   Kalam H, Fontana MF, Kumar D. 2017. Alternate splicing of transcripts shape macrophage

857   response to Mycobacterium tuberculosis infection. PLoS Pathog 13:e1006236.

858   115.   Agrawal AK, Ranjan R, Chandra S, Rout TK, Misra A, Reddy TJ. 2016. Some proteins of

859   M. tuberculosis that localise to the nucleus of THP-1-derived macrophages. Tuberculosis

860   101:75–78.

861   116.   Penn BH, Netter Z, Johnson JR, Von Dollen J, Jang GM, Johnson T, Ohol YM, Maher C,

862   Bell SL, Geiger K, Golovkine G, Du X, Choi A, Parry T, Mohapatra BC, Storck MD, Band

863   H, Chen C, Jäger S, Shales M, Portnoy DA, Hernandez R, Coscoy L, Cox JS, Krogan NJ.

864   2018. An Mtb-Human Protein-Protein Interaction Map Identifies a Switch between Host

865   Antiviral and Antibacterial Responses. Mol Cell 71:637-648.e5.

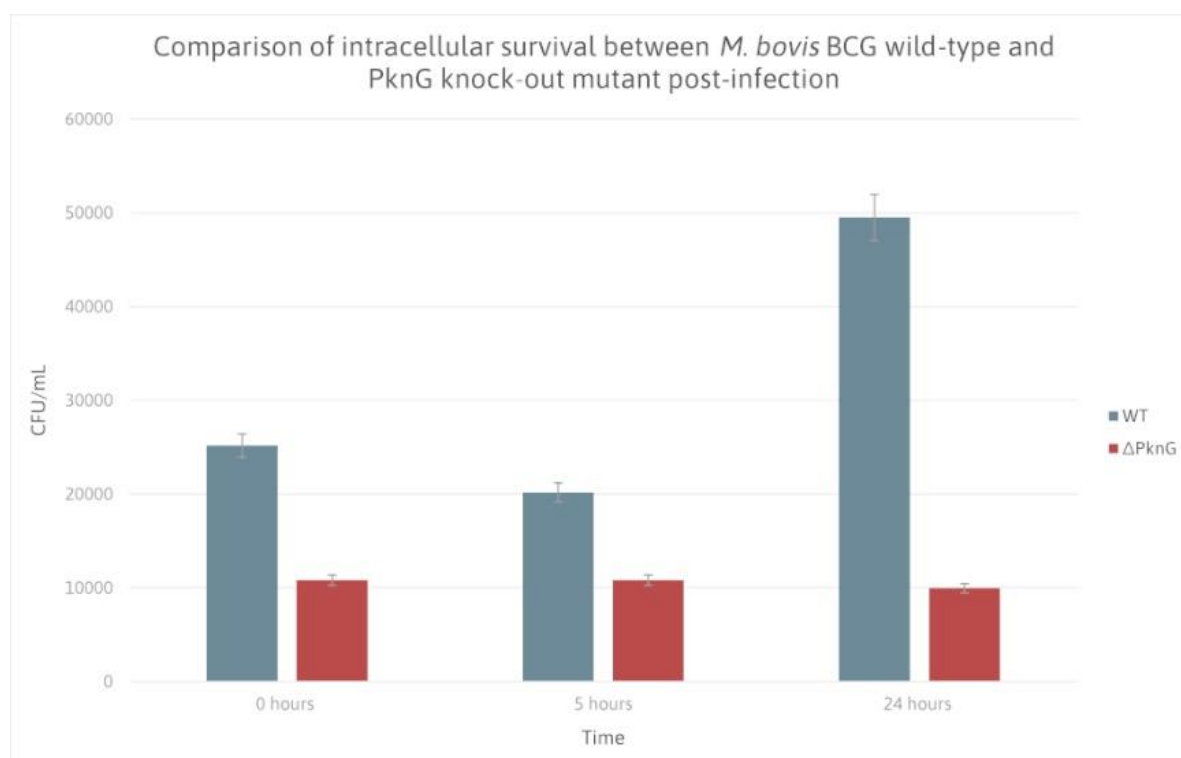866   117.   Hsu WM, Lee H, Juan HF, Shih YY, Wang BJ, Pan CY, Jeng YM, Chang HH, Lu MY, Lin

867   KH, Lai HS, Chen WJ, Tsay YG, Liao YF, Hsieh FJ. 2008. Identification of GRP75 as an

868   independent favorable prognostic marker of neuroblastoma by a proteomics analysis. Clin

869   Cancer Res 14:6237–6245.

870 118. Chalamcharla VR, Folco HD, Dhakshnamoorthy J, Grewal SIS. 2015. Conserved factor

871   Dhp1/Rat1/Xrn2 triggers premature transcription termination and nucleates

872   heterochromatin to promote gene silencing. Proc Natl Acad Sci U S A 112:15548–15555.

873 119. Tucker JF, Ohle C, Schermann G, Bendrin K, Zhang W, Fischer T, Zhang K. 2016. A Novel

874   Epigenetic Silencing Pathway Involving the Highly Conserved 5'-3' Exoribonuclease

875   Dhp1/Rat1/Xrn2 in Schizosaccharomyces pombe. PLoS Genet 12:e1005873.

876 120. Wang M, Pestov DG. 2011. 5′-end surveillance by Xrn2 acts as a shared mechanism for

877   mammalian pre-rRNA maturation and decay. Nucleic Acids Res 39:1811–1822.

878 121. Morales JC, Richard P, Patidar PL, Motea EA, Dang TT, Manley JL, Boothman DA. 2016.

879   XRN2 Links Transcription Termination to DNA Damage and Replication Stress. PLoS

880   Genet 12:e1006107.

881 122. Castro-Garza J, Luévano-Martínez ML, Villarreal-Treviño L, Gosálvez J, Fernández JL,

882   Dávila-Rodríguez MI, García-Vielma C, González-Hernández S, Cortés-Gutiérrez EI.

883   2018. Mycobacterium tuberculosis promotes genomic instability in macrophages. Mem Inst

884   Oswaldo Cruz 113:161–166.

885 123. Lochab S, Singh Y, Sengupta S, Nandicoori VK. 2020. Mycobacterium tuberculosis

886   exploits host ATM kinase for survival advantage through secA2 secretome. Elife 9:e51466.

887   **Tables**

888   **Table 1. List of differentially regulated host phosphoproteins with a minimum two-fold**

889   **increase in phosphorylation in *M. bovis* BCG WT respective to the ΔPknG mutant during**

890   **infection.**

UniProt ID	Protein name	Gene name	P-site	Log$_2$FC
F6RJ39	Apoptotic chromatin condensation inducer in the nucleus	Acin1	S937; S656; S425	2,99; 1,71; 1,71
P25799	Nuclear factor NF-kappa-B p105 subunit	Nfkb1	S447	2,99
Q922U1	U4/U6 small nuclear ribonucleoprotein Prp3	Prpf3	T469	2,53
A2AU61	RNA-binding protein Raly	Raly	S119	2,47
P15532	Nucleoside diphosphate kinase A	Nme1	T94	2,33
Q9ERG0	LIM domain and actin-binding protein 1	Lima1	S735	2,12
P27546	Microtubule-associated protein 4	Map4	S517	2,12
Q9DBR1	5'-3' exoribonuclease 2	Xrn2	S499; S501	2,05; 2,05
P70398	Probable ubiquitin carboxyl-terminal hydrolase FAF-X	Usp9x	S1600	1,77
O89053	Coronin-1A	Coro1a	T418	1,73
P49312	Heterogeneous nuclear ribonucleoprotein A1	Hnrnpa1	S6	1,72
B2RY56	RNA-binding protein 25	Rbm25	S578	1,71
Q60875	Rho guanine nucleotide exchange factor 2/ Guanine nucleotide exchange factor H1	Arhgef2	S902	1,69
Q9DBC7	cAMP-dependent protein kinase type I-alpha regulatory subunit	Prkar1a	S83	1,67
Q64337	Sequestosome-1	Sqstm1	T269; T272; T272	1,60; 1,56; 1,17
B9EJ86	Oxysterol-binding protein	Osbpl8	S314	1,56
O35601	FYN-binding protein	Fyb	S561;	1,51
P14069	Protein S100-A6	S100a6	S46	1,50
E9PUI4	Protein-methionine sulfoxide oxidase MICAL1	Mical1	T895	1,48
E9PVX6	Proliferation marker protein Ki-67	Mki67	T1159; S2392; S517	1,47; 1,32; 1,29
P84091	AP-2 complex subunit mu	Ap2m1	T156	1,45
P47754	F-actin-capping protein subunit alpha-2	Capza2	S9	1,44
F7DBB3	AHNAK nucleoprotein 2	Ahnak2	S841; T4705	1,43; 1,01
Q8CHW4	Translation initiation factor eIF-2B subunit epsilon	Eif2b5	S540	1,40
Q8C898	RIKEN cDNA C130026I21 gene	C130026I21Rik	S146	1,40
A2A8V8	Serine/arginine repetitive matrix protein 1	Srrm1	S878	1,32
Q9DBJ1	Phosphoglycerate mutase 1	Pgam1	S14	1,31
O08583	THO complex subunit 4	Alyref	S237	1,29
E3UVT8	Anion exchange protein	Slc4a7	S1052; S23	1,29; 1,26
Q61029	Lamina-associated polypeptide 2, isoforms beta/delta/epsilon/gamma	Tmpo	S183	1,27
Q6ZQ58	La-related protein 1	Larp1	S743	1,27
Q8JZQ9	Eukaryotic translation initiation factor 3 subunit B	Eif3b	S79	1,26
Z4YKC4	Eukaryotic translation initiation factor 4 gamma 3	Eif4g3	S274	1,23
Q05D44	Eukaryotic translation initiation factor 5B	Eif5b	S215	1,23
Q8BZN6	Dedicator of cytokinesis protein 10	Dock10	S877; T1440; S1257	1,08
Q8CIH5	1-phosphatidylinositol 4,5-bisphosphate phosphodiesterase gamma-2	Plcg2	Y759	1,14
Q8CBW3	Abl interactor 1	Abi1	S183	1,09
Q62376	U1 small nuclear ribonucleoprotein 70 kDa	Snrnp70	S226	1,07
A2A5R2	Brefeldin A-inhibited guanine nucleotide-exchange protein 2	Arfgef2	S227	1,06
Q569Z6	Thyroid hormone receptor-associated protein 3	Thrap3	S248; S253; S243	1,05; 1,05; 1,03
P62482	Voltage-gated potassium channel subunit beta-2	Kcnab2	S14	1,05
Q78ZA7	Nucleosome assembly protein 1-like 4	Nap1l4	S125	1,04
E9Q616	AHNAK nucleoprotein (desmoyokin)	Ahnak	T4705	1,01
Q8C3J5	Dedicator of cytokinesis protein 2	Dock2	S1729	1,00

891 **Figures and Figure Legends**

892

Comparison of intracellular survival between *M. bovis* BCG wild-type and PknG knock-out mutant post-infection

893 **Figure 1. Survival of *M. bovis* BCG WT and ΔPknG mutant in macrophages at different time**

894 **points post-infection.** Histogram showing the bacterial growth of the different mycobacterial

895 strains in RAW 264.7 macrophages at 0 hours, 5 hours, and 24 hours post-infection.
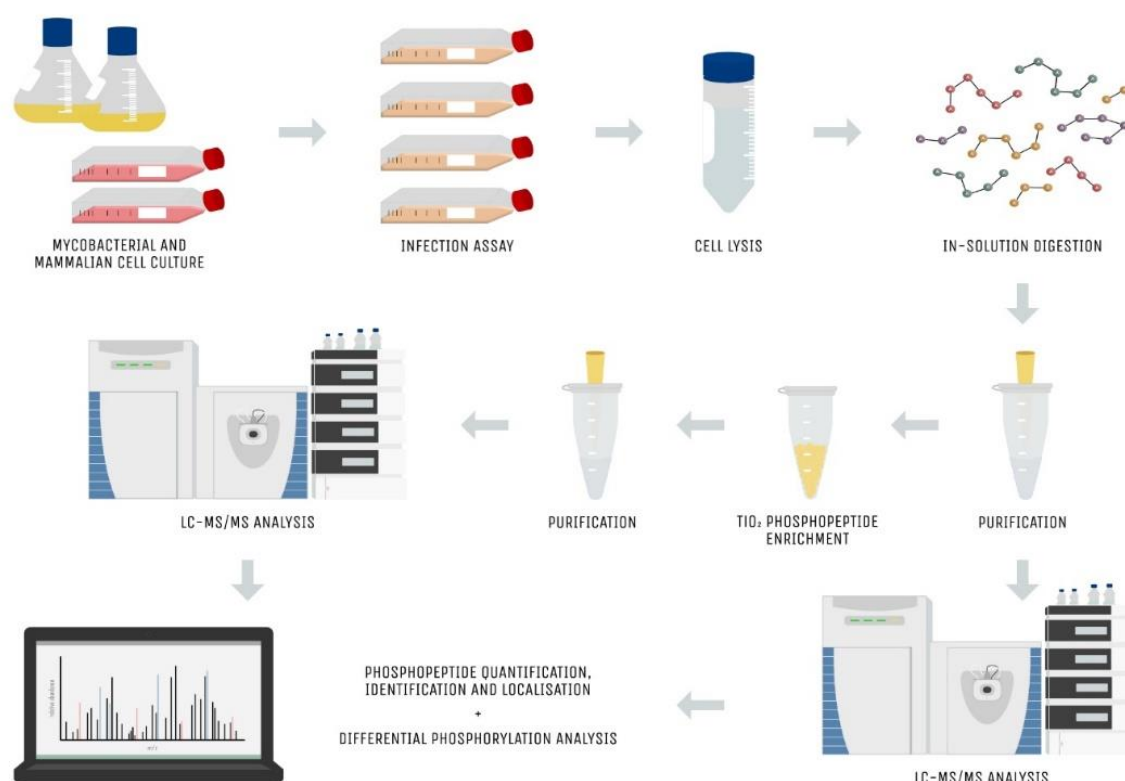
896

Figure 2. Proteomic and phosphoproteomic workflow used in this study. *M. bovis* BCG wild-type and ΔPknG strains were grown until mid-log phase and RAW 264.7 cells were cultured in D10 media until confluent. Infection assays were carried out at MOI 1:4 with a one-hour incubation. The RAW 264.7 cells were washed and lysed in the presence of protease and phosphatase inhibitors, followed by in-solution digestion with Lys-C and Trypsin. The samples were purified using reverse-phase C18 chromatography and an aliquot reserved for proteome analysis. Phosphopeptides were enriched using TiO_2 phosphopeptide enrichment kit, followed by another clean-up step. LC-MS/MS data acquisition was then performed on an HPLC coupled to a Q Exactive mass spectrometer. The raw data files were processed using MaxQuant and analysed using Perseus and other software packages.

907

Figure 3. Analysis of quantified phosphopeptides. (A) Volcano plot highlighting the significantly differentially phosphorylated peptides. Scatter plot showing the phosphopeptide log2 fold-change (WT/ΔPknG) plotted against the -log10(p-value) highlighting the differentially phosphorylated peptides (two-sample t-test with BH FDR <0.05). Down-regulated and up-regulated phosphopeptides in the presence of PknG are indicated in red and green, respectively. **(B) Hierarchical clustering analysis of differentially up-regulated phosphopeptides in the presence of PknG.** Heatmap showing the abundance levels and clustering of the significantly differentially unregulated phosphopeptides (two-sample t-test with BH FDR <0.05; log2FC ≥1 WT/ΔPknG). Phosphopeptide intensities up-regulated are coloured green while down-regulated are coloured red. Row headings represent gene names and column headings represent samples.
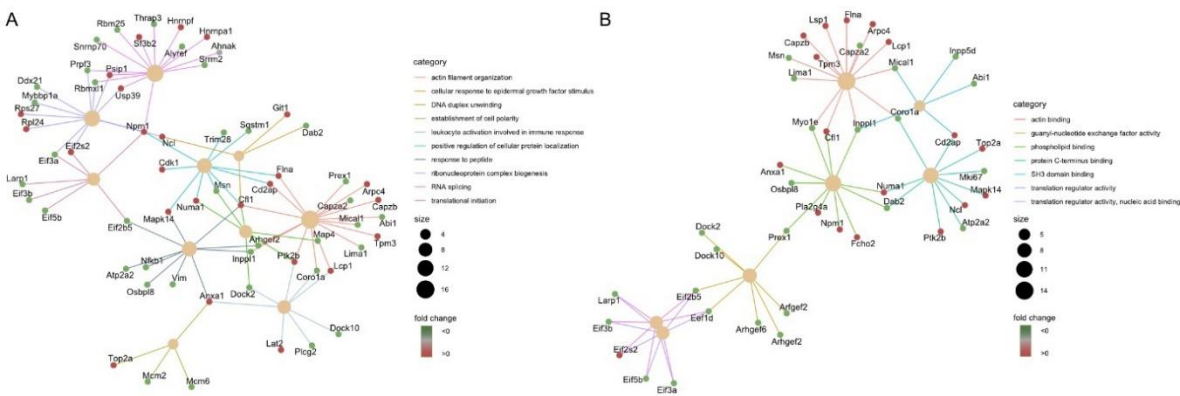
918

Figure 4. Functional enrichment network of differentially phosphorylated proteins in the presence of mycobacterial PknG associated with up to 10 most significant GO (A) biological processes and (B) molecular functions. Nodes are coloured according to fold change and sized according to the number of associated proteins.
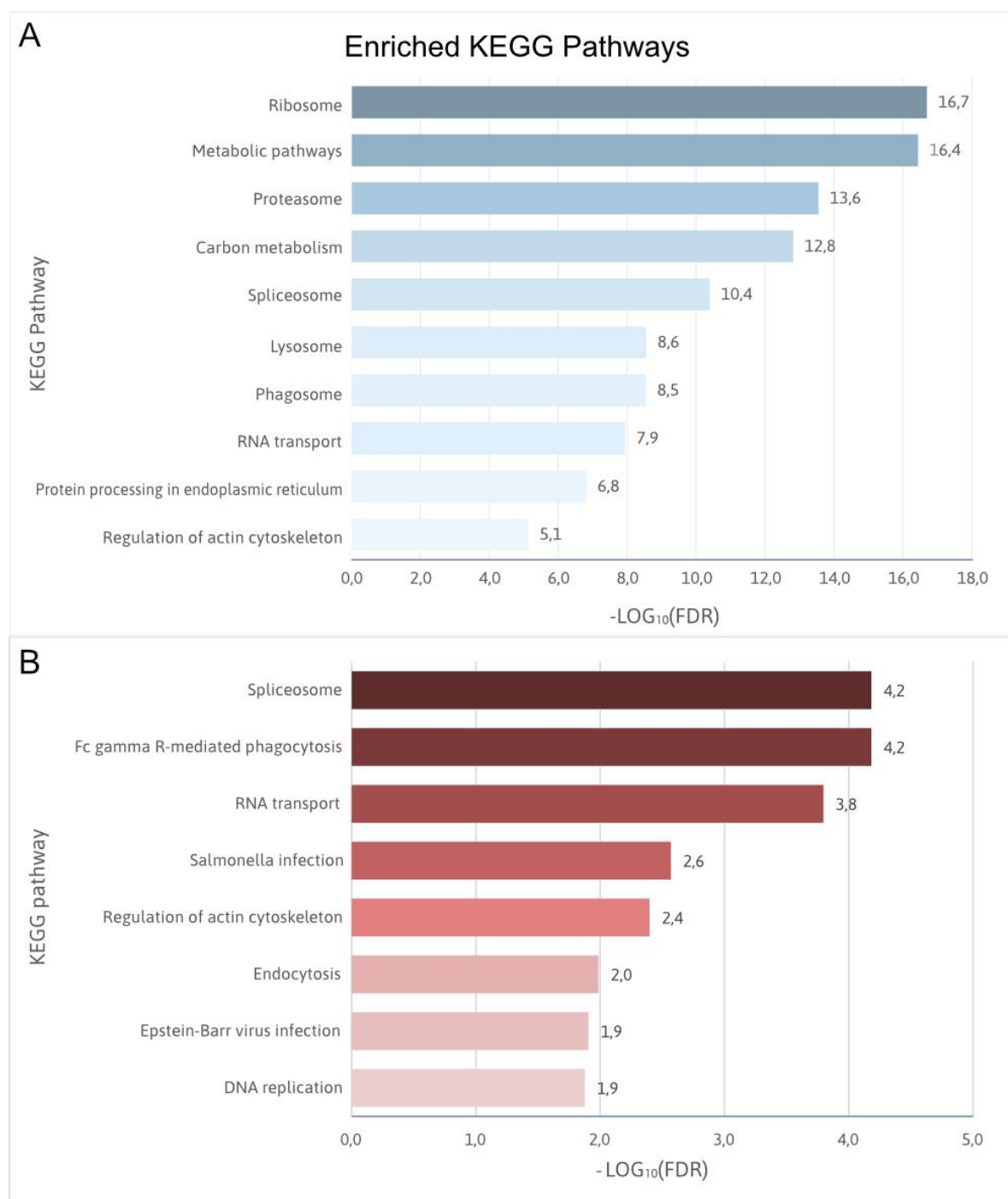
923

Figure 5. Significantly enriched KEGG pathways of differentially abundant (A) proteins and (B) phosphoproteins. Bar charts ranking the significant Kyoto Encyclopaedia of Genes and Genomes (KEGG) pathways retrieved after functional enrichment analysis of the differentially regulated proteins and phosphoproteins in the presence of PknG during mycobacterial infection.

928
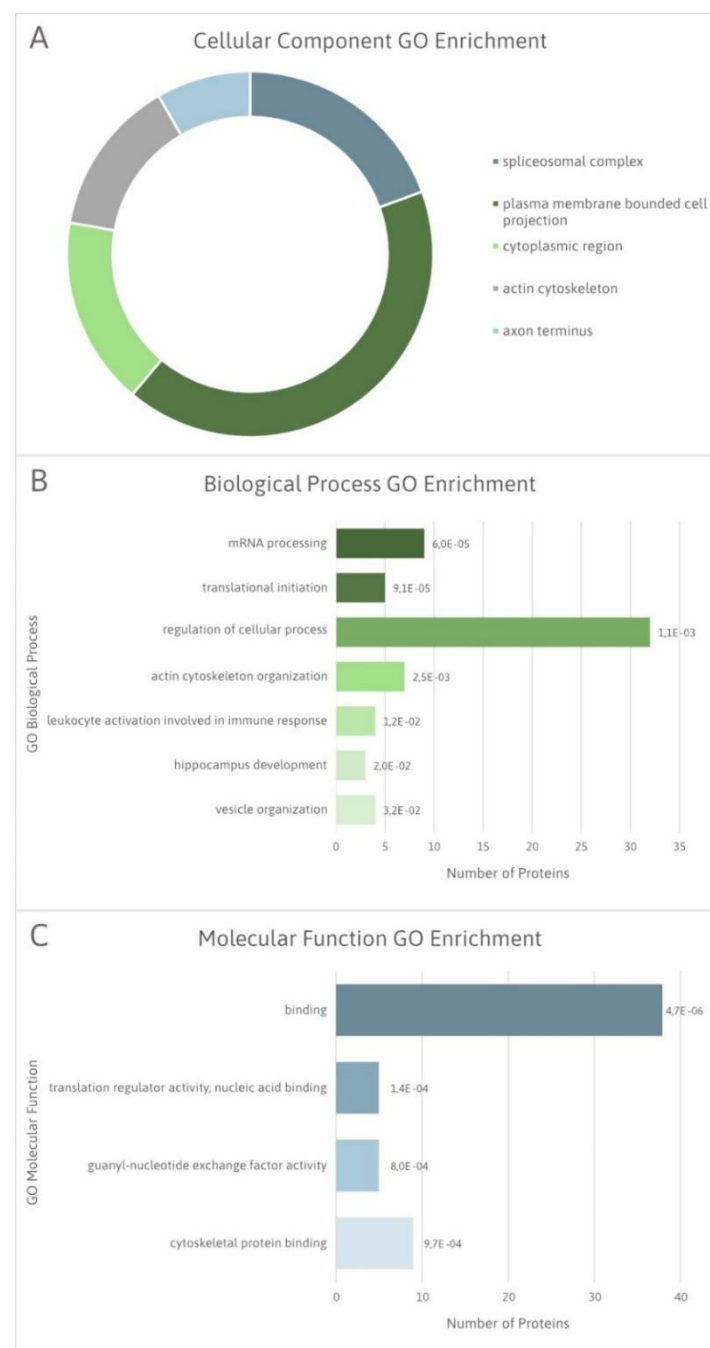
Figure 6. Significantly enriched GO terms of candidate host macrophage substrates of mycobacterial PknG. (A) Pie chart illustrating the significantly enriched cellular component GO terms of the candidate host PknG substrates. **(B)** Bar chart ranking of the significantly enriched biological process GO terms, and **(C)** molecular function GO terms of the candidate host PknG substrates. Data labels represent FDR values for each enriched GO term.
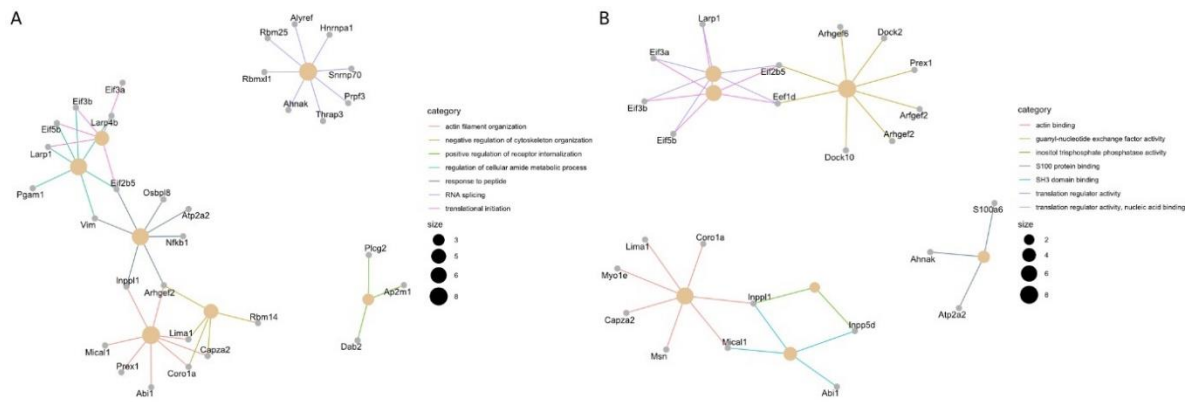
934

Figure 7. Functional enrichment network of differentially up-regulated phosphoproteins in the presence of PknG associated with significant GO (A) biological processes and (B) molecular functions. Nodes are sized according to the number of associated proteins.